# Resonance fluorescence and absorption spectra from a two-level atom driven by coherent and stochastic fields

Peng Zhou* and S. Swain†
*Department of Applied Mathematics and Theoretical Physics, Queen's University of Belfast, Belfast BT7 1NN, Northern Ireland, United Kingdom*
(Received 3 June 1998)

The steady-state populations, the fluorescent intensity-intensity correlation function, and the resonance fluorescence and absorption spectra of a two-level atom bichromatically driven by a strong, coherent field and a weak, stochastic field with tunable carrier frequency and wide bandwidth are investigated analytically. Surprisingly, the population is inverted if the stochastic field is appropriately detuned from the coherent field, which is assumed resonant with the atomic transition. The resonance fluorescence spectrum still displays a three-peaked structure, but with linewidths and heights that depend upon the frequency and bandwidth of the stochastic field as well as the intensities of both fields. Asymmetric fluorescence spectra are found when the coherent field is detuned from the atomic resonance frequency. The intensity-intensity correlation function varies dramatically with the carrier frequency of the stochastic field. For appropriate choices of the parameters, the fluorescent emission of the atom is antibunched for all time. The absorption spectral features also deviate significantly from those of the monochromatically driven atom. By appropriately tuning the stochastic field, one finds that a sharp peak (absorption) or hole (gain) can occur at line center and the probe beam can be amplified at either the lower-frequency Rabi sideband or the higher-frequency sideband and the inversionless gain can be enhanced. [S1050-2947(98)00612-X]

PACS number(s): 42.50.Hz, 42.50.Dv, 32.80.−t

## I. INTRODUCTION

The study of resonance fluorescence and probe absorption spectra has provided much fundamental insight into the subject of atom-light interactions. It is well known that when a two-level atom is driven by a strong laser beam, the fluorescence spectrum exhibits a Mollow triplet [1], in which the sidebands are symmetrically shifted from the laser frequency by the generalized Rabi frequency and are one and a half times as wide and one-third as high as the central peak. The relative widths and heights of the triplet are independent of the intensity of the laser field. The probe absorption spectrum of such a system also shows a similar three-resonance structure [2].

Recently, considerable attention has been paid to modifying the standard Mollow spectrum. Indeed, there are many ways to achieve this. One method is to bathe the atom in a squeezed vacuum. Carmichael *et al.* [3] then predicted a phase-sensitive Mollow triplet in this case when the atom is strongly driven, whereas, for intermediate driving intensities, Swain [4] reported anomalous spectral features: hole burning and dispersive profiles at line center. Another method is to place the atom inside a cavity, when a wide variety of spectral features, such as dynamical suppression and enhancement and spectral line narrowing [5–8] of the Mollow triplet, has been predicted, as well as the existence of multipeaked spectral profiles [8,9]. If the atom is driven by a bichromatic coherent field instead of a monochromatic laser, the spectrum also differs qualitatively from the standard Mollow triplet, displaying a series of symmetric sidebands with intensity-independent peak separations, intensity-dependent peak heights, and alternating spectral linewidths [10].

On the other hand, from the experimental point of view, it is important to take account of the fact that the coherent driving field may undergo phase and amplitude fluctuations. For an atom driven by such a finite bandwidth laser, spectral broadening, sideband suppression, and asymmetry [11–13] of the Mollow spectrum are predicted. Interestingly, Vemuri *et al.* [14] have recently shown that a stochastic field with arbitrary bandwidth, when added to the coherent driving field, may give rise to dramatic narrowing of the linewidths of all three peaks, depending on the central frequency of the stochastic field. Their studies, however, are largely based on numerical calculations. In this paper we consider a limited situation in which the atom is driven by a strong coherent field and a weak stochastic field with a wide bandwidth, where analytical evaluations can be performed, without neglecting any essential physical processes. We find that, besides those phenomena predicted by Vemuri *et al.* [14], population inversion, photon antibunching, a narrow absorption peak at line center, and enhancement of the inversionless gain can be also achieved.

With this model we can eliminate the stochastic field to obtain a master equation for the reduced density matrix of the atom: The stochastic field effectively forms a reservoir. The interesting feature here, though, is that the properties of the reservoir turn out to depend strongly on the difference between the coherent and stochastic field center frequencies. We have a reservoir whose properties are easily modified and these modifications in turn strongly affect such physical properties as the inversion and intensity-intensity correlation function as mentioned in the abstract.

Our paper is organized as follows. In Sec. II we consider

*Electronic address: peng@qo1.am.qub.ac.uk
†Electronic address: s.swain@qub.ac.uk

 

the interaction of a two-level atom with a colored field consisting of a coherent part with an additional stochastic component. An effective master equation for the reduced density operator of the atom is derived when the coherent driving field is much stronger than the stochastic part. In Sec. III we show that, for certain frequencies of the stochastic field, the population may be inverted. We study the resonance fluorescence spectrum of such an atom in Sec. IV. Asymmetrically spectral features and spectral line narrowing are predicted. The effect of the stochastic field on the second-order correlation function of the fluorescent field is discussed in Sec. V. By appropriately tuning the coherent and stochastic fields, one finds that the fluorescent photons emitted from the atom are completely antibunched. Section VI is devoted to the probe absorption spectrum. We find that the presence of the additionally stochastic field may give rise to spectral asymmetries, a narrowed spectral line at line center, and inversionless gain enhancement. We present conclusions in Sec. VII.

## II. MODEL

We consider a single two-level atom with transition frequency $\omega_A$, bichromatically driven by a coherent field with a frequency $\omega_L$ and a constant amplitude $E_c$ as well as by a stochastic field with a central frequency $\omega_s$ and a complex, stochastically fluctuating amplitude $E_s(t)$. The atom is also damped by the electromagnetic vacuum. In a frame rotating at the frequency $\omega_L$ the master equation of the density matrix operator $\rho$ for the system is of the form

$$\dot{\rho}=-i[H_{a\text{-}c}+H_{a\text{-}s},\rho]+\gamma(2\sigma_-\rho\sigma_+-\sigma_+\sigma_-\rho-\rho\sigma_+\sigma_-), \tag{1}$$

where

$$H_{a\text{-}c}=\frac{\Delta}{2}\sigma_z+\frac{\Omega}{2}(\sigma_++\sigma_-), \tag{2}$$

$$H_{a\text{-}s}=\frac{1}{2}[x(t)e^{-i\delta t}\sigma_++x^*(t)e^{i\delta t}\sigma_-], \tag{3}$$

where $H_{a\text{-}c}$ and $H_{a\text{-}s}$ describe the interaction of the atom with the coherent field and the stochastic field respectively, $\gamma$ is the atomic decay constant, $\Delta=\omega_A-\omega_L$ is the detuning of the atomic resonance frequency and the frequency of the coherent part of the driving field, $\delta=\omega_s-\omega_L$ denotes the frequency difference between the coherent and stochastic components of the driving field, $\Omega=2|\mathbf{d}\cdot\mathbf{e}E_c|/\hbar$ is the Rabi frequency of the coherent field, and $x(t)=2\mathbf{d}\cdot\mathbf{e}E_s(t)/\hbar$ represents the stochastic amplitude of the atom–stochastic-field interaction, which is assumed to be a complex Gaussian-Markovian random process with zero mean value and correlation functions [12–14]

$$\langle x(t)x^*(t')\rangle=D\kappa e^{-\kappa|t-t'|}, \tag{4a}$$

$$\langle x(t)x(t')\rangle=0, \tag{4b}$$

where $D$ is the strength of the stochastic process and $\kappa$ can be associated with the bandwidth of the stochastic field. These first-order correlation functions (4a) and (4b) describe a field undergoing both phase and amplitude fluctuations, which result in a finite bandwidth $\kappa$ of the field [12–14]. In the limit $\kappa\to\infty$, the correlation (4a) reduces to a $\delta$ function and the stochastic field is then a complex white noise field.

For the general situation, the model must be numerically solved [14]. In this paper we are interested in the case where the intensity of the coherent part is much greater than that of the stochastic field and the bandwidth $\kappa$ of the stochastic field is much greater than the atomic linewidth (in other words, the correlation time $\kappa^{-1}$ of the stochastic field is very short compared to the radiative lifetime $\gamma^{-1}$ of the atom), i.e.,

$$\Omega\gg\sqrt{D\kappa},\quad \kappa\gg\gamma. \tag{5}$$

In this limit one can invoke standard perturbative techniques to eliminate the stochastic variable $x(t)$ [6,7]. Consequently, the master equation for the reduced density operator $\rho$ takes the atom

$$\dot{\rho}=-i[H_{a\text{-}c},\rho]-\frac{1}{4}([\sigma_-,[S_+,\rho]]+[\sigma_+,[S_-,\rho]])+\gamma(2\sigma_-\rho\sigma_+-\sigma_+\sigma_-\rho-\rho\sigma_+\sigma_-), \tag{6}$$

where

$$\begin{aligned}S_-&=D\kappa\int_0^\infty d\tau\, e^{-(\kappa+i\delta)\tau}e^{-iH_{a\text{-}c}\tau}\sigma_-e^{iH_{a\text{-}c}\tau}\\&=\mathcal{A}_0\sigma_z+\mathcal{A}_1\sigma_++\mathcal{A}_2\sigma_-,\\S_+&=(S_-)^\dagger\\&=\mathcal{A}_0^*\sigma_z+\mathcal{A}_1^*\sigma_-+\mathcal{A}_2^*\sigma_+,\end{aligned} \tag{7}$$

with

$$\begin{aligned}\mathcal{A}_0&=\frac{D\kappa\Omega}{4\bar{\Omega}^2}\left[\frac{2\Delta}{\kappa+i\delta}-\frac{\bar{\Omega}+\Delta}{\kappa+i(\delta-\bar{\Omega})}+\frac{\bar{\Omega}-\Delta}{\kappa+i(\delta+\bar{\Omega})}\right],\\\mathcal{A}_1&=\frac{D\kappa\Omega^2}{4\bar{\Omega}^2}\left[\frac{2}{\kappa+i\delta}-\frac{1}{\kappa+i(\delta-\bar{\Omega})}-\frac{1}{\kappa+i(\delta+\bar{\Omega})}\right],\\\mathcal{A}_2&=\frac{D\kappa}{4\bar{\Omega}^2}\left[\frac{2\Omega^2}{\kappa+i\delta}+\frac{(\bar{\Omega}+\Delta)^2}{\kappa+i(\delta-\bar{\Omega})}+\frac{(\bar{\Omega}-\Delta)^2}{\kappa+i(\delta+\bar{\Omega})}\right],\end{aligned} \tag{8}$$

and $\bar{\Omega}=\sqrt{\Omega^2+\Delta^2}$ is a generalized Rabi frequency. The first term on the right-hand-side of Eq. (6) represents atomic stimulated emission and absorption by the coherent part of the driving field, while the second term is associated with the effect of the stochastic part of the driving field. It is apparent that the effect of the stochastic field on the atom consists of an incoherent decay and an incoherent pumping. The last term represents the vacuum-induced incoherent decay of the atom. It is rather surprising that the master equation (6) is formally similar to that of a coherently driven atom coupled to a frequency-tunable cavity mode in the bad cavity limit [6,7].

Obviously, the coefficients $\mathcal{A}_0, \mathcal{A}_1, \mathcal{A}_2$ are Rabi frequency dependent and resonant when the central frequency of the stochastic field is tuned to $\delta = 0, \pm\bar{\Omega}$. The resonance property reflects the fact that the atom–coherent-field interaction forms a ''dressed'' atom [15] whose energy-level structure is intensity dependent and whose spontaneous emission dominates at the three frequencies $\omega_L, \omega_L \pm \bar{\Omega}$. The dressed atom is then driven by the stochastic field. Therefore, when the central frequency of the stochastic field is tuned to these three frequencies, the corresponding atomic transition is enhanced. In the remaining part we shall mainly focus on the effects of the frequencies of the coherent and stochastic fields on the populations and spectra of the driven atom, i.e., we fix the intensities of both fields and the bandwidth of the stochastic field, but keep the frequencies of both fields tunable.

### III. POPULATION INVERSION

From the master equation (6) one can obtain the Bloch equations, which govern the atomic evolution, in the form

$$\langle \dot{\sigma}_+ \rangle = -\left( \gamma - i\Delta + \frac{\mathcal{A}_2^*}{2} \right) \langle \sigma_+ \rangle + \frac{\mathcal{A}_1^*}{2} \langle \sigma_- \rangle - \frac{i\Omega}{2} \langle \sigma_z \rangle, \tag{9}$$

$$\langle \dot{\sigma}_z \rangle = -\gamma_z \langle \sigma_z \rangle + (\mathcal{A}_0 - i\Omega) \langle \sigma_+ \rangle + (\mathcal{A}_0^* + i\Omega) \langle \sigma_- \rangle - 2\gamma,$$

where $\gamma_z = 2\gamma + \mathrm{Re}(\mathcal{A}_2)$ is the decay rate of the population, which is now dependent not only on the atomic spontaneous decay constant but also on the Rabi frequency of the coherent field and the bandwidth and carrier frequency of the stochastic field. In the steady state, the population difference $\langle \sigma_z \rangle$ is determined by

$$\langle \sigma_z \rangle_s = -\frac{2\gamma}{\gamma_z + \beta}, \tag{10}$$

where

$$\beta = \frac{i\Omega}{2} \frac{(\mathcal{A}_0 - i\Omega)\left[ \gamma + i\Delta + \frac{1}{2}(\mathcal{A}_2 - \mathcal{A}_1^*) \right] - (\mathcal{A}_0^* + i\Omega)\left[ \gamma - i\Delta + \frac{1}{2}(\mathcal{A}_2^* - \mathcal{A}_1) \right]}{\left| \gamma + i\Delta + \frac{1}{2}\mathcal{A}_2 \right|^2 - \frac{1}{4}|\mathcal{A}_1|^2}. \tag{11}$$

When both the fields are resonant with the atomic transition, i.e., $\Delta = 0$ and $\delta = 0$, it is easy to see that

$$\beta = \frac{\Omega^2}{2\gamma + D} \left( 2 + \frac{D\kappa}{\kappa^2 + \Omega^2} \right). \tag{12}$$

Therefore, $\langle \sigma_z \rangle_s$ is always negative. This differs from the case of a resonantly driven atom coupled to a resonant cavity mode, where the population is inverted if the intensity of the driving field is very high [7].

However, if the frequency of the stochastic field is appropriately detuned from the atomic transition frequency, population inversion can be achieved. See, for example, in Fig. 1, where the parameters are taken to be $\kappa = 100$, $D = 40$, $\gamma = 1$, and $\Delta = 0$. [For simplicity, all parameters are measured in units of $\gamma$ (i.e., $\gamma = 1$) throughout the paper.] For $\Omega = 500$ (dashed line) the population is inverted in the regime $176.6 < |\delta| < 432.6$, while inversion occurs over the range $297.4 < |\delta| < 955$ for the Rabi frequency $\Omega = 1000$ (solid line). The population difference $\langle \sigma_z \rangle_s$ as a function of the Rabi frequency $\Omega$ and the stochastic-field frequency $\delta$ for the two coherent-field frequencies $\Delta = 0$ and 100 is shown in Figs. 2 and 3, respectively. The former figure clearly demonstrates population inversion over certain carrier frequencies of the stochastic field. With increasing Rabi frequency $\Omega$, the population tends to distribute evenly over the ground and excited states.

These plots also clearly display the dependence of the population on the carrier frequency of the stochastic field. The resonances take place at $\delta = 0$ and $\delta = \pm\bar{\Omega}$. The resonance profiles, however, are determined by the detuning be-

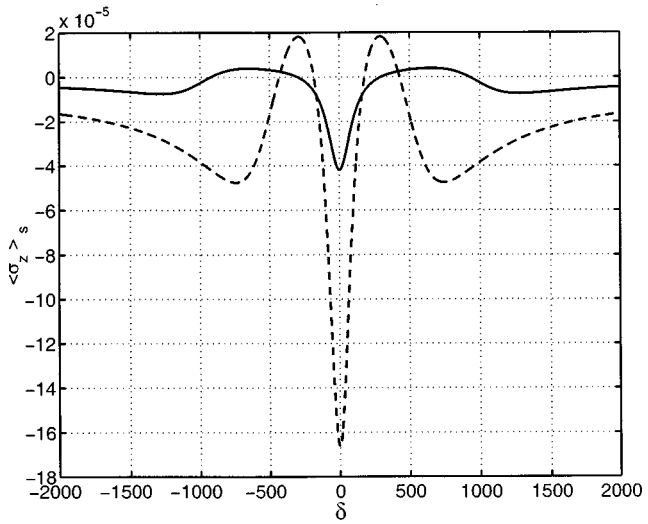


FIG. 1. Steady-state population difference $\langle \sigma_z \rangle_s$ as a function of the detuning $\delta$ between the coherent and stochastic fields for the parameters $\kappa = 100$, $D = 40$, $\gamma = 1$, $\Delta = 0$, and different intensities of the coherent field, $\Omega = 500$ (dashed line) and 1000 (solid line). (All parameters are measured in units of $\gamma$, that is, we set $\gamma = 1$ throughout these figures.)

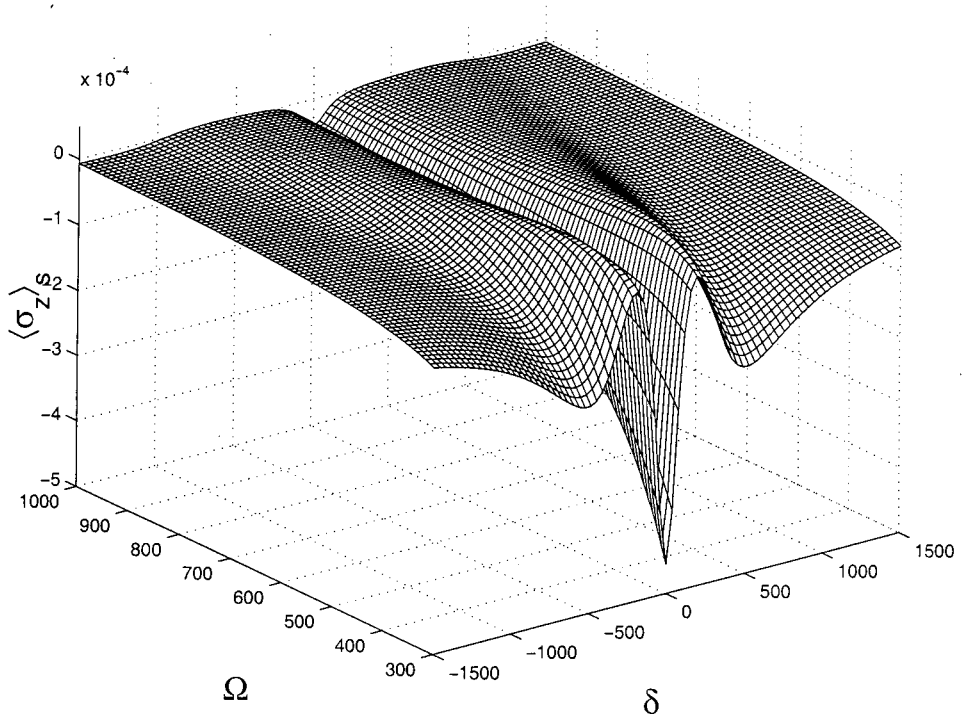


FIG. 2. Same as Fig. 1, but a three-dimensional plot with $\Delta = 0$.

tween the atom and the coherent field. For a resonant coherent driving field (see Figs. 1 and 2) the resonance line shapes of the atomic population are Lorentzian shaped at $\delta = 0$ and Rayleigh-wing shaped at $\delta = \pm\Omega$, respectively. In contrast, for a nonresonant coherent driving field, shown in Fig. 3, the resonance profile is Rayleigh-wing shaped at $\delta = 0$ and Lorentzian shaped at $\delta = \pm\Omega$. The stochastic field frequency dependence of the population may be confirmed by recording the atomic fluorescence intensity against the frequency of the stochastic field.

## IV. RESONANCE FLUORESCENCE SPECTRUM

The incoherent fluorescence spectrum of the atom can be expressed in terms of the two-time correlation of the atomic operators as

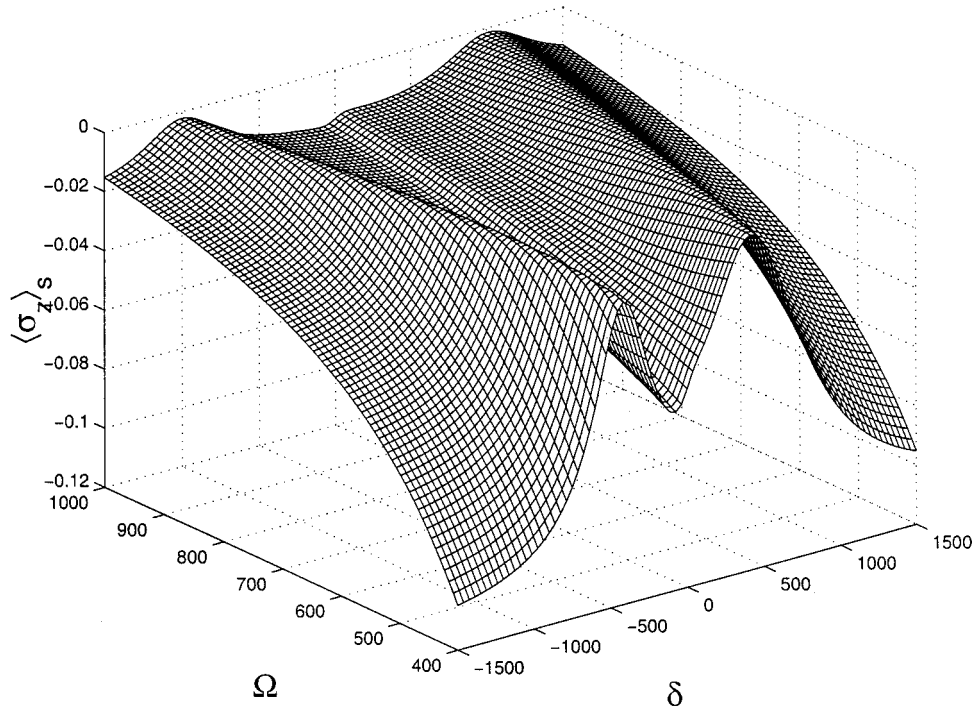


FIG. 3. Same as Fig. 2, but with $\Delta = 100$.

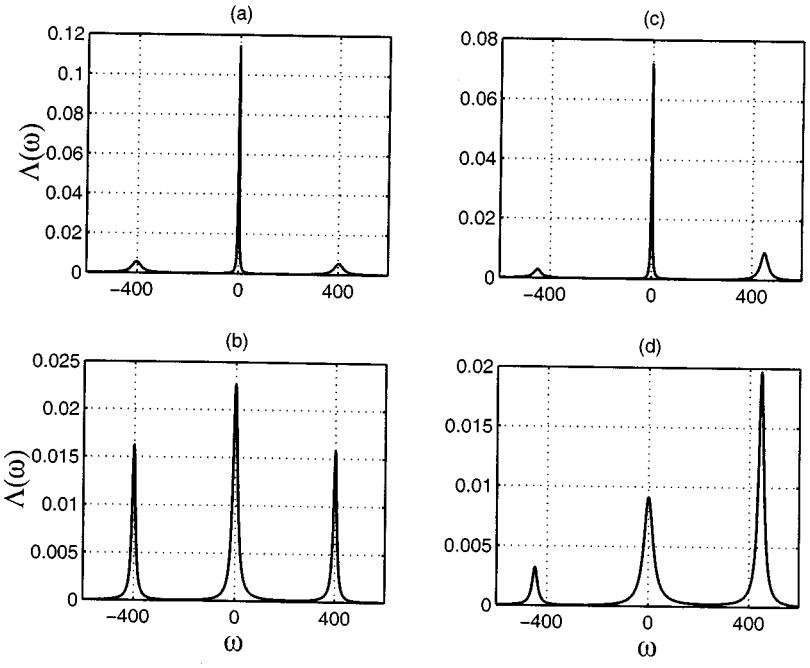


FIG. 4. Incoherent resonance fluorescence spectrum $\Lambda(\omega)$ for the parameters $\Omega=400$, $\kappa=100$, $D=40$, $\gamma=1$, and various frequencies of the coherent and stochastic fields: (a) $\Delta=0$, $\delta=0$, (b) $\Delta=0$, $\delta=\overline{\Omega}$, (c) $\Delta=200$, $\delta=0$, and (d) $\Delta=200$, $\delta=\overline{\Omega}$.

$$\Lambda(\omega)=\mathrm{Re}\int_0^\infty \lim_{t\to\infty}\langle\sigma_+(t),\sigma_-(t+\tau)\rangle e^{i\omega\tau}d\tau$$
$$=\mathrm{Re}\left[\frac{M(z)}{N(z)}\right]_{z=-i\omega}, \tag{13}$$

where

$$M(z)=\left[(z+\gamma_z)\left(z+\gamma-i\Delta+\frac{\mathcal{A}_2^*}{2}\right)+\frac{i\Omega}{2}(\mathcal{A}_0-i\Omega)\right]\alpha_1$$
$$+\frac{1}{2}[(z+\gamma_z)\mathcal{A}_1+i\Omega(\mathcal{A}_0-i\Omega)]\alpha_2$$
$$+\frac{i\Omega}{2}\left(z+\gamma-i\Delta+\frac{\mathcal{A}_2^*-\mathcal{A}_1}{2}\right)\alpha_3, \tag{14}$$

$$N(z)=(z+\gamma_z)\left[\left(z+\gamma+i\Delta+\frac{\mathcal{A}_2}{2}\right)\right.$$
$$\left.\times\left(z+\gamma-i\Delta+\frac{\mathcal{A}_2^*}{2}\right)-\frac{1}{4}\left|\mathcal{A}_1\right|^2\right]$$
$$-\frac{i\Omega}{2}(\mathcal{A}_0^*+i\Omega)\left(z+\gamma-i\Delta+\frac{\mathcal{A}_2^*-\mathcal{A}_1}{2}\right)$$
$$+\frac{i\Omega}{2}(\mathcal{A}_0-i\Omega)\left(z+\gamma+i\Delta+\frac{\mathcal{A}_2-\mathcal{A}_1^*}{2}\right), \tag{15}$$

with

$$\alpha_1=\frac{1}{2}(1+\langle\sigma_z\rangle_s)-|\langle\sigma_+\rangle_s|^2,$$
$$\alpha_2=-\langle\sigma_+\rangle_s^2, \tag{16}$$
$$\alpha_3=-(1+\langle\sigma_z\rangle_s)\langle\sigma_+\rangle_s,$$

where $\langle\sigma_+\rangle_s$ and $\langle\sigma_z\rangle_s$ are the steady-state solution of the Bloch equation (9).

Figure 4 exhibits the effects of the frequencies of the coherent and stochastic fields on the resonance fluorescence spectrum for $\Omega=400$, $\kappa=100$, $D=40$, and $\gamma=1$. When the coherent field is in resonance with the atom, i.e., $\Delta=0$, the fluorescence spectrum is symmetric, as depicted in Figs. 4(a) and 4(b), whereas asymmetric fluorescence spectra are displayed in Figs. 4(c) and 4(d) for $\Delta=200$, that is, when the coherent field is detuned from the atom. The spectral features, however, vary dramatically with the frequency of the stochastic field. For example, if the frequency of the stochastic field is the same as that of the coherent field, $\delta=0$, as shown in Figs. 4(a) and 4(c), the central peak is much higher and narrower than the sidebands. When the stochastic field is tuned to one of the Rabi sidebands however, the central peak is suppressed and broadened while the sidebands are enhanced and narrowed. See Figs. 4(b) and 4(d). This agrees with the predictions of Vemuri *et al.* [14] using Monte Carlo simulation techniques.

We plot three dimensional spectra for $\Omega=400$, $\kappa=100$, $D=40$, and $\gamma=1$ in Figs. 5 ($\Delta=0$) and 6 ($\Delta=200$) to further demonstrate the dependence of the three peaks on the carrier frequency of the stochastic field. Figure 5 shows a symmetric spectral profile with the central peak being enhanced at $\delta=0$ and suppressed at $\delta=\pm\Omega$ and the sideband peaks having minima at $\delta=0$ and maxima at $\delta=\pm 248.6$.

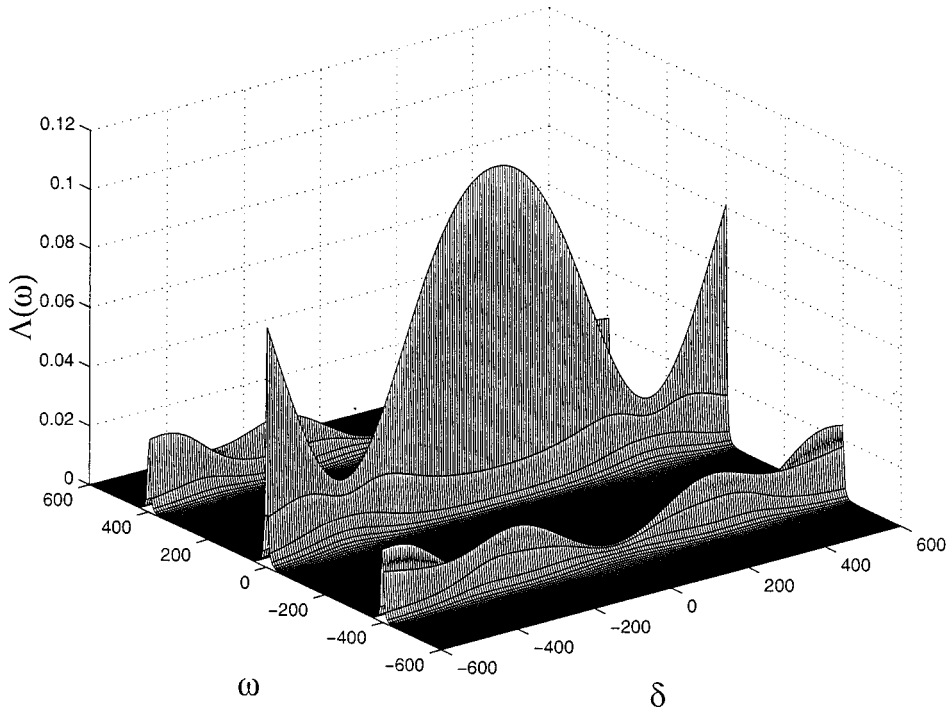


FIG. 5. Same as Fig. 4, but a three-dimensional plot with $\Delta=0$.

Figure 6 displays an asymmetric fluorescence spectrum of the atom driven by a nonresonant coherent field. The low-frequency sideband is suppressed over wide ranges of the stochastic field frequency in the case of $\Delta=200$.

The physics associated with the narrowing and asymmetries of the stochastic-field-modified Mollow spectrum can be easily explored by working in the basis of the semiclassical dressed states $|\pm\rangle$, defined by the eigenvalue equation $H_{a\text{-}c}|\pm\rangle=\pm(\bar{\Omega}/2)|\pm\rangle$. They are associated with the bare atomic states $|0\rangle,|1\rangle$ through the expressions

$$|+\rangle=s|0\rangle+c|1\rangle, \quad |-\rangle=c|0\rangle-s|1\rangle, \tag{17}$$

where

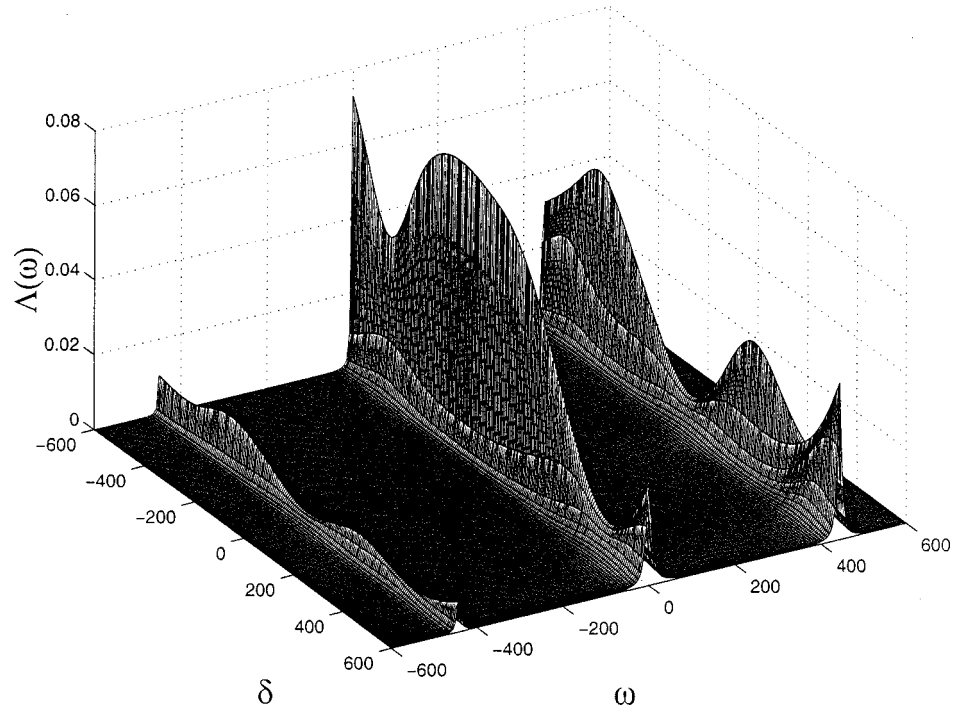


FIG. 6. Same as Fig. 5, but with $\Delta=200$.

$$c=\sqrt{\frac{\bar{\Omega}+\Delta}{2\bar{\Omega}}},\quad s=\sqrt{\frac{\bar{\Omega}-\Delta}{2\bar{\Omega}}}. \tag{18}$$

If the condition $\bar{\Omega}\gg\kappa$ holds, the contributions from terms with different resonance frequencies are negligibly small and the secular approximation is thus valid [15]. The optical Bloch equations then simplify to

$$\begin{aligned}\langle\dot{\Pi}_{+-}\rangle&=-(\Gamma_\perp-i\bar{\Omega}-i\Omega_{sh})\langle\Pi_{+-}\rangle,\\ \langle\dot{\Pi}_z\rangle&=-\Gamma_\parallel\langle\Pi_z\rangle-2\gamma(c^2-s^2),\end{aligned} \tag{19}$$

where $\Pi_{+-}=|+\rangle\langle-|$ is the dressed-state transition operator, $\Pi_z=(\Pi_{++}-\Pi_{--})$ with $\Pi_{\pm\pm}=|\pm\rangle\langle\pm|$ being the population operator of the dressed state $|\pm\rangle$, and

$$\begin{aligned}\Gamma_\perp&=\gamma(1+2c^2s^2)+\frac{D}{2}\kappa^2\left[\frac{4c^2s^2}{\kappa^2+\delta^2}\right.\\ &\left.+\frac{s^4}{\kappa^2+(\delta+\bar{\Omega})^2}+\frac{c^4}{\kappa^2+(\delta-\bar{\Omega})^2}\right],\\ \Gamma_\parallel&=2\gamma(c^4+s^4)+D\kappa^2\left[\frac{s^4}{\kappa^2+(\delta+\bar{\Omega})^2}+\frac{c^4}{\kappa^2+(\delta-\bar{\Omega})^2}\right],\\ \Omega_{sh}&=\frac{D}{2}\kappa\left[\frac{s^4(\delta+\bar{\Omega})}{\kappa^2+(\delta+\bar{\Omega})^2}-\frac{c^4(\delta-\bar{\Omega})}{\kappa^2+(\delta-\bar{\Omega})^2}\right].\end{aligned} \tag{20}$$

$\Gamma_\perp,\Gamma_\parallel$ indicate the decay rate of the dressed-state polarization and of the dressed-state population inversion, respectively, while $\Omega_{sh}$ is a frequency shift from the generalized Rabi frequency $\bar{\Omega}$. All these parameters are resonant when the frequency of the stochastic field is tuned to the center and sidebands of the Mollow spectrum.

The incoherent resonance fluorescence spectrum in the dressed state basis then takes the form

$$\begin{aligned}\Lambda(\omega)&=\frac{4c^2s^2\Gamma_\parallel\langle\Pi_{--}\rangle_s\langle\Pi_{++}\rangle_s}{\Gamma_\parallel^2+\omega^2}+\frac{c^4\Gamma_\perp\langle\Pi_{++}\rangle_s}{\Gamma_\perp^2+(\omega-\bar{\Omega}-\Omega_{sh})^2}\\ &+\frac{s^4\Gamma_\perp\langle\Pi_{--}\rangle_s}{\Gamma_\perp^2+(\omega+\bar{\Omega}+\Omega_{sh})^2}.\end{aligned} \tag{21}$$

Obviously, the central spectral line with width $2\Gamma_\parallel$ results from atomic downward transitions between the same dressed states of two adjacent dressed-state doublets and is proportional to $\langle\Pi_{--}\rangle_s\langle\Pi_{++}\rangle_s$. The left-hand sideband, however, is due to downward transitions from the substate $|-\rangle$ of one dressed-state doublet to the substate $|+\rangle$ of the next dressed-state doublet and is associated with the population $\langle\Pi_{--}\rangle_s$ of the dressed state $|-\rangle$. The right-hand sideband originates from the downward transitions $|+\rangle\rightarrow|-\rangle$ between two nearlying dressed-state doublets and is proportional to $\langle\Pi_{++}\rangle_s$. Both sidebands have the same linewidth $2\Gamma_\perp$.

In the case of $\Delta=0$, that is, the coherent driving field is resonant with the atom, $c=s=1/\sqrt{2}$, the population is equally distributed over both dressed states; therefore, the fluorescence spectrum is symmetric, regardless of the carrier frequency of the stochastic field. Varying the frequency, however, dramatically modifies the spectral linewidths and heights. For instance, for the stochastic field resonant with the atom and the coherent field, $\delta=0$, Eq. (20) then reduces to

$$\begin{aligned}\Gamma_\perp&=\frac{3\gamma}{2}+\frac{D}{2}\left[1+\frac{1}{2}\frac{\kappa^2}{\kappa^2+\Omega^2}\right],\\ \Gamma_\parallel&=\gamma+\frac{D}{2}\frac{\kappa^2}{\kappa^2+\Omega^2}.\end{aligned} \tag{22}$$

It is clear that the heights and linewidths of the spectrum are Rabi frequency dependent, which is qualitatively different from the free-space Mollow triplet [1]. Increasing the Rabi frequency results in central spectral line narrowing. For $\Omega\gg\kappa$, the central linewidth $2\Gamma_\parallel$ is approximately $2\gamma$, while the sideband linewidth is $3\gamma+D$, that is, the sidebands are widened. The ratio of the central peak height to the sideband height is also enlarged by the factor $3+D/\gamma$, instead of the factor 3 in the standard Mollow triplet [1,15]. See, for example, Fig. 4(a).

If we tune the frequency of the stochastic field to resonance with the Mollow sidebands, $\delta=\pm\Omega$, then Eq. (20) gives rise to

$$\begin{aligned}\Gamma_\perp&=\frac{3\gamma}{2}+\frac{D}{8}\left[1+\frac{4\kappa^2}{\kappa^2+\Omega^2}+\frac{\kappa^2}{\kappa^2+4\Omega^2}\right],\\ \Gamma_\parallel&=\gamma+\frac{D}{4}\left[1+\frac{\kappa^2}{\kappa^2+4\Omega^2}\right].\end{aligned} \tag{23}$$

The central peak is broadened while the sidebands are significantly narrowed, compared to those of $\delta=0$, e.g., in the frame 4(b). The higher the intensity of the coherent field, the narrower the sideband linewidth. In the limit of $\Omega\gg\kappa$ and $D\gg\gamma$, the sidebands can be narrower than the central peak (i.e., $\Gamma_\perp<\Gamma_\parallel$). The ratio of the central peak to the sideband is reduced by $(12\gamma+D)/(4\gamma+D)$; therefore, the three peaks have similar heights for $D\gg\gamma$.

If the frequency of the coherent field is detuned from the atom resonance frequency, i.e., $\Delta\neq0$, one sees from Eq. (19) that the populations of the dressed states $|\pm\rangle$ are unequal and thus the spectrum is asymmetric, unlike the case of the monochromatically driven two-level atom [1], where the Mollow triplet is always symmetric.

## V. INTENSITY-INTENSITY CORRELATION

The intensity-intensity correlation function $g^{(2)}(t)$ of the fluorescence field is defined as

$$g^{(2)}(t)=\frac{\langle\sigma_+(0)\sigma_+(t)\sigma_-(t)\sigma_-(0)\rangle_s}{\langle\sigma_+(0)\sigma_-(0)\rangle_s^2}. \tag{24}$$

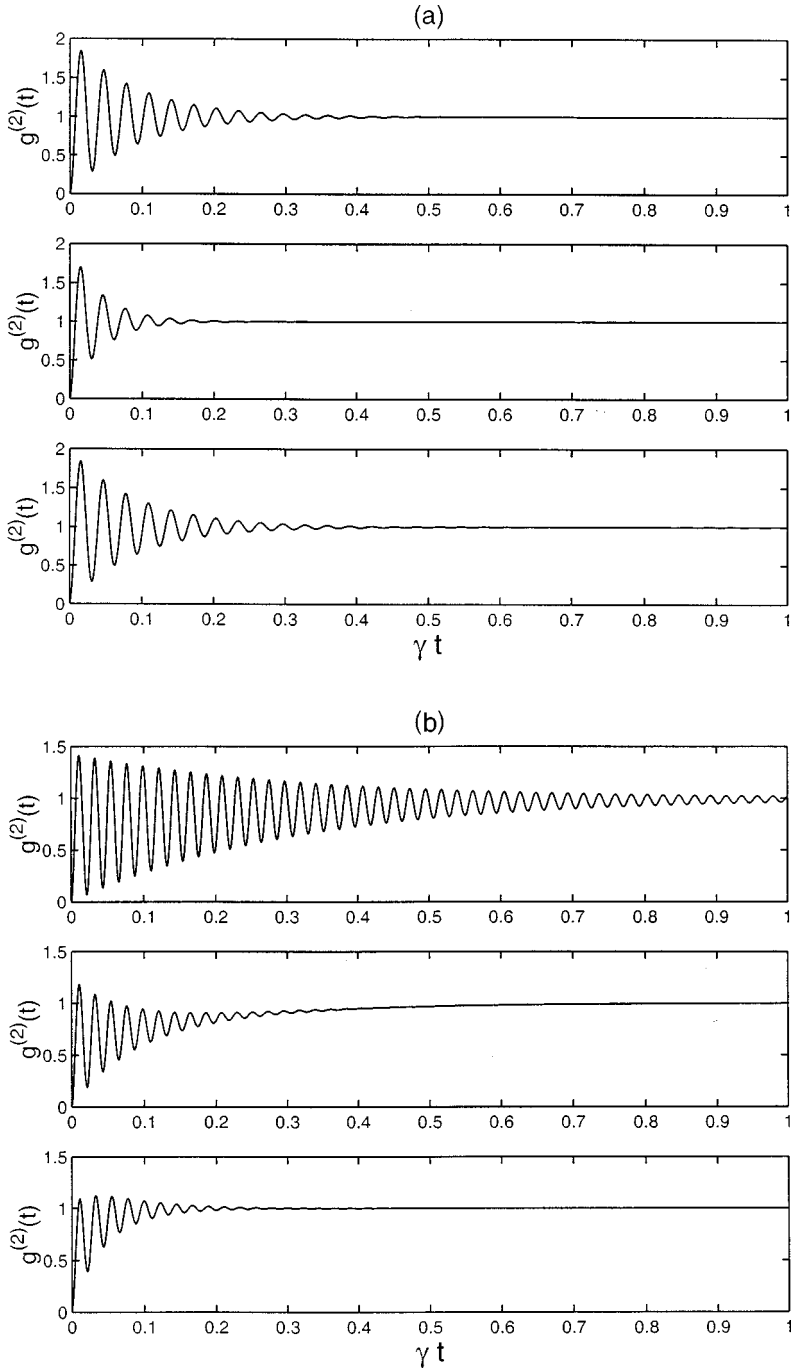


FIG. 7. Intensity-intensity correlation function $g^{(2)}(t)$ for the parameters $\Omega=200$, $\kappa=100$, $D=40$, $\gamma=1$, and (a) $\Delta=0$, (b) $\Delta=200$, and (c) $\Delta=500$. From the top frame to the bottom one, the frequency of the stochastic field is taken to be $\delta=-\overline{\Omega},0,\overline{\Omega}$, respectively.

It is related to the intensity fluctuations of the fluorescence field and contains information about the probability of detecting a fluorescent photon at time $t$ given that one was detected at time 0.

Figures 7 present the intensity-intensity correlation function $g^{(2)}(t)$ for $\Omega=200$, $\kappa=100$, $D=40$, $\gamma=1$, and various frequencies of the coherent laser and the stochastic field: (a) $\Delta=0$, (b) $\Delta=200$, and (c) $\Delta=500$, with the values $\delta=-\overline{\Omega},0,\overline{\Omega}$ displayed from the top to bottom frames, respectively. This figure clearly shows that the photon correlation varies dramatically with the carrier frequencies of the stochastic and coherent fields. For $\Delta=0$, that is, the coherent field is resonant with the atomic transition, the correlation function is identical when the frequency of the stochastic field is tuned to either Rabi sideband of the Mollow triplet, but it differs when the frequency of the stochastic field is tuned to the Mollow center. The oscillations in the latter reach their steady-state value of unity more quickly than the others.

When the coherent field is detuned from the atomic transition frequency, $\Delta\neq 0$, the second-order correlation functions $g^{(2)}(t)$ corresponding to the different stochastic frequencies, $\delta=-\overline{\Omega},0,\overline{\Omega}$, are not identical. For example, for $\Delta>0$ in Figs. 7(b) and 7(c), the oscillation decay rate of

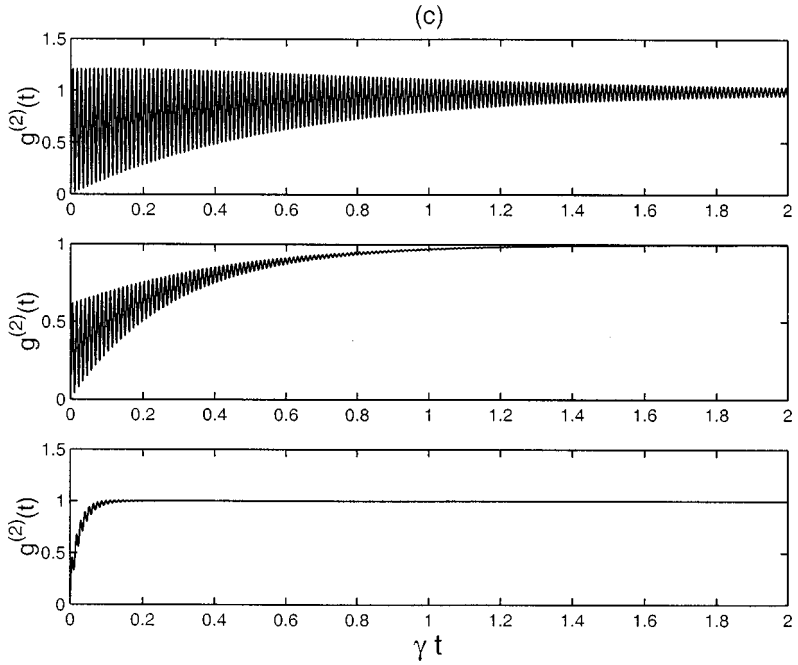


FIG. 7. (*Continued*).

$g^{(2)}(t)$ for $\delta=-\overline{\Omega}$ is less than that for $\delta=0$, which in turn is less than that for $\delta=\overline{\Omega}$. In other words, the time for the oscillations to decay to their steady-state value decreases as the stochastic field-atom detuning changes from $\delta=-\overline{\Omega}$ to 0 and then to $\overline{\Omega}$. The latter two cases can exhibit complete photon antibunching, i.e., $g^{(2)}(t)<1$ for all $t$, if the coherent field-atom detuning is very large, e.g., in Fig. 7(c), where $\Delta=500$.

The photon antibunching of the fluorescence field from a monochromatically, coherently driven two-level atom was predicted and observed decades ago [16], for weak Rabi frequencies ($\Omega\leqslant\gamma$). The antibunched fluorescence predicted here, however, occurs in the strong Rabi frequency regime ($\Omega\gg\gamma$), where $g^{(2)}(t)$ oscillates strongly and persists for a long time before reaching the same steady-state value as in the absence of the stochastic field.

As we work in the regime in which the coherent field is so strong that the secular approximation is valid, we may simply express the photon correlation function as

$$g^{(2)}(t)=1-\frac{(c^2-s^2)^2(\Gamma_\parallel-2\gamma)}{\Gamma_\parallel-2\gamma(c^2-s^2)^2}e^{-\Gamma_\parallel t}-\frac{4c^2s^2\Gamma_\parallel}{\Gamma_\parallel-2\gamma(c^2-s^2)^2}e^{-\Gamma_\perp t}\cos(\overline{\Omega}+\Omega_{sh})t. \tag{25}$$

Obviously, the correlation function oscillates at the frequency $\overline{\Omega}+\Omega_{sh}\simeq\overline{\Omega}$, which barely depends on the stochastic field [noting that $\Omega_{sh}$ is negligibly small in the limit (5)]. The amplitudes of the oscillations decrease exponentially at rates $\Gamma_\parallel,\Gamma_\perp$ which are, respectively, the decay rates of the dressed population and coherence, and depend on the frequencies and intensities of both the coherent and stochastic fields.

When the coherent field is resonant with the atom, $\Delta=0$, Eq. (25) reads

$$g^{(2)}(t)=1-e^{-\Gamma_\perp t}\cos(\overline{\Omega}+\Omega_{sh})t, \tag{26}$$

where the magnitude of the oscillations decays at the rate $\Gamma_\perp$. From Eqs. (22) and (23) we see that when $\delta=\pm\Omega$ the rate is less than that for $\delta=0$ and therefore the oscillations in the former case last longer, as indicated in Fig. 7(a).

When the coherent field is far off resonant with the atom, say, $\Delta\gg\Omega$ for example, then $(c^2-s^2)^2=(\Delta/\overline{\Omega})^2\simeq 1, 4c^2s^2=(\Omega/\overline{\Omega})^2\ll 1, c^4\simeq 1$, and $s^4\simeq 0$. The photon correlation function $g^{(2)}(t)$ [Eq. (25)] is approximately of the form

$$g^{(2)}(t)\simeq 1-\left(\frac{\Delta}{\overline{\Omega}}\right)^2 e^{-\Gamma_\parallel t}-\left(\frac{\Omega}{\overline{\Omega}}\right)^2\left(1+\frac{2\gamma}{D\eta}\right)\times e^{-\Gamma_\perp t}\cos(\overline{\Omega}+\Omega_{sh})t, \tag{27}$$

where

$$\eta=\left(\frac{\kappa}{2\overline{\Omega}}\right)^2,\quad \Gamma_\perp\simeq\gamma+\frac{D}{2}\left(\frac{\kappa}{2\overline{\Omega}}\right)^2,$$

$$\Gamma_\parallel\simeq 2\gamma+D\left(\frac{\kappa}{2\overline{\Omega}}\right)^2 \quad \text{when} \quad \delta=-\overline{\Omega}, \tag{28}$$

$$\eta=\left(\frac{\kappa}{\overline{\Omega}}\right)^2,\quad \Gamma_\perp\simeq\gamma+\frac{D(\Omega^2+\kappa^2)}{2\overline{\Omega}^2},$$

$$\Gamma_\parallel\simeq 2\gamma+D\left(\frac{\kappa}{\overline{\Omega}}\right)^2 \quad \text{when} \quad \delta=0, \tag{29}$$

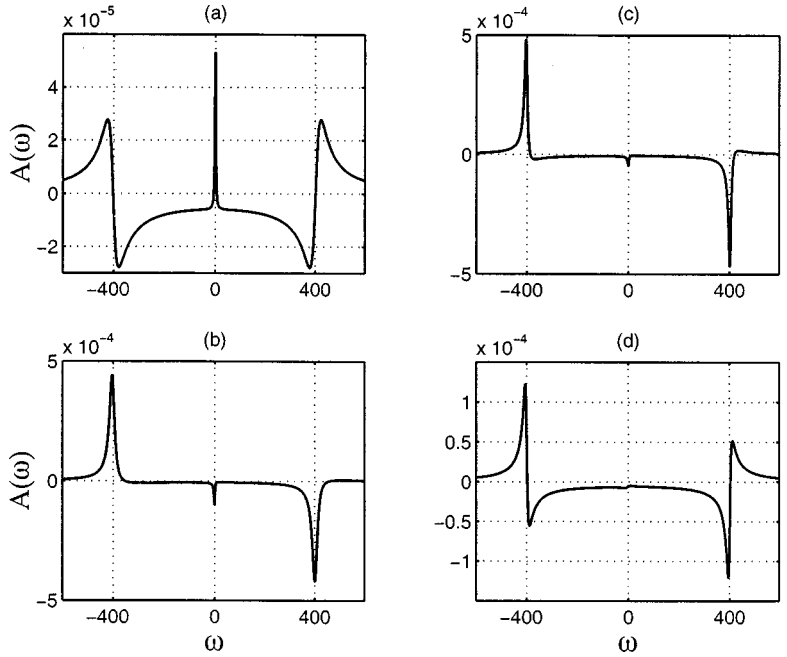


FIG. 8. Probe absorption spectrum $A(\omega)$ for the parameters $\Omega=400$, $\kappa=100$, $D=40$, $\gamma=1$, $\Delta=0$ and various frequencies of the stochastic fields: (a) $\delta=0$, (b) $\delta=100$, (c) $\delta=200$, and (d) $\delta=\overline{\Omega}$.

$$\eta=1, \quad \Gamma_{\perp}\simeq\gamma+\frac{D}{2}, \quad \Gamma_{\parallel}\simeq 2\gamma+D \quad \text{when} \quad \delta=\overline{\Omega}. \tag{30}$$

The oscillations of the correlation function thus reach the steady-state value 1 at different time scales for various frequencies of the stochastic field. The larger the $\Gamma_{\perp}, \Gamma_{\parallel}$ the more quickly $g^{(2)}(t)$ reaches 1. See, for instance, in Fig. 7(c).

The expression (27) also clearly shows the effect of the strength $D$ of the stochastic field on the intensity-intensity correlation of the fluorescent field. If $D$ is very small, $g^{(2)}(t)$ may be greater than 1 for certain times. However, for $D\eta \gg \gamma$, the values of $g^{(2)}(t)$ is always less than 1, that is, the fluorescence emission exhibits the complete photon antibunching effect. This is illustrated in the middle and bottom frames of Fig. 7(c).

## VI. ABSORPTION SPECTRUM

The steady-state absorption spectrum of a frequency tunable, very weak, probe field is proportional to the Fourier transform of the stationary average value of the two-time commutator of the atomic raising and lowering operators:

$$A(\omega)=\mathrm{Re}\int_0^{\infty}\lim_{t\to\infty}\langle[\sigma_-(t+\tau),\sigma_+(t)]\rangle e^{i\omega\tau}d\tau, \tag{31}$$

where $\omega=\omega_{probe}-\omega_L$ is the frequency of the probe beam measured from the driving laser frequency. Again, invoking the quantum regression theorem together with the optical Bloch equations (9), one may calculate the two-time correlation function $\langle[\sigma_-(\tau),\sigma_+(0)]\rangle$. The absorption spectrum is formally the same as Eq. (13), but with

$$\alpha_1=-\langle\sigma_z\rangle_s, \qquad \alpha_2=0, \qquad \alpha_3=2\langle\sigma_+\rangle_s. \tag{32}$$

We show the probe absorption spectra in Fig. 8 for $\Omega=400$, $\kappa=100$, $D=40$, $\gamma=1$, $\Delta=0$, and different frequencies of the stochastic field: (a) $\delta=0$, (b) $\delta=100$, (c) $\delta=200$, and (d) $\delta=400$. It is clear from Fig. 8(a) that when the frequency of the stochastic field is tuned to the central line of the Mollow triplet, the central component exhibits a Lorentzian line shape, while the sidebands show the Rayleigh-wing line shape. Inversionless gain occurs over the range $0<|\omega|<\Omega$. These features are quite similar to that of probe absorption in a coherently driven atom [2,17]. However, there is a narrow absorption peak at line center (at the atomic resonant transition frequency), unlike that in the monochromatically driven atom where the probe beam is transparent at this frequency. When the stochastic field is significantly detuned from the coherent field (atomic resonance frequency), for example, $\delta=100$ in Fig. 8(b) and $\delta=200$ in Fig. 8(c), all resonance line shapes are, however, Lorentzian-like. The probe beam may be amplified not only at the higher-frequency sideband but also at line center, without the help of population inversion. [Note that for the parameters taken in Figs. 8(a), 8(b), and 8(d), the population difference is negative: $\langle\sigma_z\rangle_s<0$. Although $\langle\sigma_z\rangle_s=1.0192\times10^{-5}$ for the parameters in Fig. 8(c), probe gain is mainly attributed to the effect of the carrier frequency of the stochastic field.] Comparing with the gain when $\delta=0$, the inversionless gain is also enhanced by appropriately detuning both driving fields. When the stochastic field is resonant with the higher-frequency Rabi sideband, all three components display dispersivelike (Rayleigh-wing) profiles with the center component being negligibly small: See, for example, Fig. 8(d). Probe gain without inversion

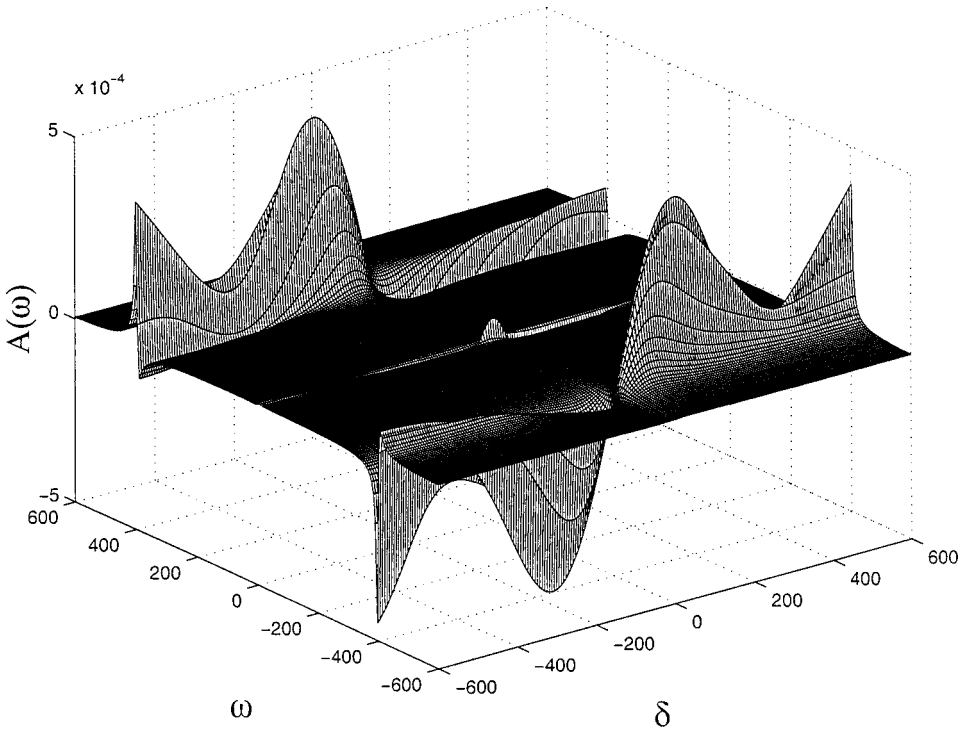


FIG. 9. Same as Fig. 8, but a three-dimensional plot with $\Delta=0$.

takes place over the range $-\Omega<\delta<\Omega$ and the gain near the higher-frequency sideband is stronger than that near the lower-frequency sideband.

Figures 9 and 10 present three-dimensional absorption spectra for $\Omega=400$, $\kappa=100$, $D=40$, $\gamma=1$, and $\Delta=0,200$, respectively. The absorption spectra are asymmetric, except for $\Delta=0$ and $\delta=0$. In the case where the coherent field is tuned to resonance with the atomic transition, $\Delta=0$, as in Fig. 9 for example, the probe beam can be amplified at the higher-frequency Rabi sideband when the carrier frequency of the stochastic field exceeds the frequency of the coherent field, i.e., $\delta>0$, while probe gain occurs at the lower-frequency Rabi sideband when $\delta<0$. Another qualitatively different feature from the standard absorption spectrum is that gain can take place at the atomic transition frequency (spectral line center) for a properly tuned stochastic field. In the case of $\Delta>0$, for instance $\Delta=200$ in Fig. 10, the probe beam is amplified at the lower-frequency Rabi sideband while it is

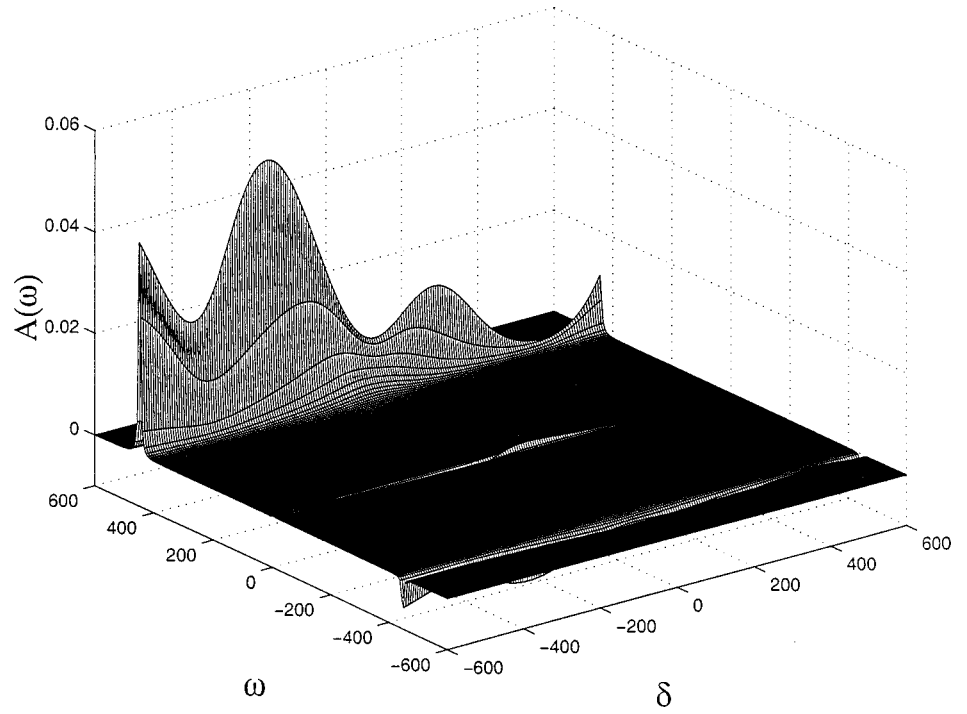


FIG. 10. Same as Fig. 9, but with $\Delta=200$.

absorbed at the higher-frequency sideband, regardless of the frequency of the stochastic field. However, probe absorption or gain at line center (the frequency of the coherent field) is strongly dependent on values of $\delta$. For $\delta>0$ the probe beam is absorbed at line center while it is amplified at this frequency if $\delta<0$. When $\Delta<0$, these spectral features are reversed.

## VII. CONCLUSIONS

We investigate the modifications of the steady-state population, resonance fluorescence and absorption spectra, and fluorescent intensity-intensity correlation of a two-level atom driven by a strong, coherent field with an additional, weak stochastic field with tunable carrier frequency and wide bandwidth. We have shown that the stochastic field effectively forms a reservoir, whose properties may be engineered simply by changing its center frequency. A variety of effects are predicted, including population inversion, photon antibunching, spectral linewidth narrowing and broadening, and spectral height suppression and enhancement. All these predictions are strongly dependent upon the carrier frequency of the stochastic field. We also show that the inversionless gain can be enhanced by appropriately tuning the stochastic field. The current study provides a clear physical picture of a fluctuating field interacting with a strongly, coherently driven atom.

## ACKNOWLEDGMENT

This work was supported by the United Kingdom EPSRC.

[1] B. R. Mollow, Phys. Rev. **188**, 1969 (1969); F. Y. Wu, R. E. Grove, and S. Ezekiel, Phys. Rev. Lett. **35**, 1426 (1997); For reviews see, for example, S. Swain, Adv. At. Mol. Phys. **16**, 159 (1980); B. R. Mollow, Prog. Opt. **19**, 1 (1981).

[2] B. R. Mollow, Phys. Rev. A **5**, 2217 (1972); F. Y. Wu, S. Ezekiel, M. Ducloy, and B. R. Mollow, Phys. Rev. Lett. **38**, 1077 (1977).

[3] H. J. Carmichael, A. S. Lane, and D. F. Walls, Phys. Rev. Lett. **58**, 2539 (1987); J. Mod. Opt. **34**, 821 (1987).

[4] S. Smart and S. Swain, Phys. Rev. A **48**, R50 (1993); S. Swain, Phys. Rev. Lett. **73**, 1493 (1994); S. Swain and P. Zhou, Phys. Rev. A **52**, 4845 (1995).

[5] M. Lewenstein, T. W. Mossberg, and R. J. Glauber, Phys. Rev. Lett. **59**, 775 (1987); M. Lewenstein and T. W. Mossberg, Phys. Rev. A **37**, 2048 (1988); Y. Zhu, A. Lezama, and T. W. Mossberg, Phys. Rev. Lett. **61**, 1946 (1988); A. Lezama, Y. Zhu, S. Morin, and T. W. Mossberg, Phys. Rev. A **39**, R2754 (1989).

[6] W. Lange and H. Walther, Phys. Rev. A **48**, 4551 (1993); G. S. Agarwal, W. Lange, and H. Walther, *ibid*. **48**, 4555 (1993).

[7] P. Zhou and S. Swain, Phys. Rev. A **58**, 1515 (1998).

[8] T. Quang and H. Freedhoff, Phys. Rev. A **47**, 2285 (1993); H. Freedhoff and T. Quang, Phys. Rev. Lett. **72**, 474 (1994); H. Freedhoff and T. Quang, J. Opt. Soc. Am. B **10**, 1337 (1993); **12**, 9 (1995).

[9] J. I. Cirac, H. Ritsch, and P. Zoller, Phys. Rev. A **44**, 4541 (1991); M. Loffler, G. M. Meyer, and H. Walther, *ibid*. **55**, 3923 (1997).

[10] Y. Zhu, Q. Wu, A. Lezama, D. J. Gauthier, and T. W. Mossberg, Phys. Rev. A **41**, R6574 (1990); H. S. Freedhoff and Z. Chen, *ibid*. **41**, 6013 (1990); G. S. Agarwal, Y. Zhu, D. J. Gauthier, and T. W. Mossberg, J. Opt. Soc. Am. B **8**, 1163 (1991); Z. Ficek and H. S. Freedhoff, Phys. Rev. A **48**, 3092 (1993); **53**, 4275 (1996).

[11] (a) G. S. Agarwal, Phys. Rev. Lett. **37**, 1383 (1976); (b) J. H. Eberly, *ibid*. **37**, 1387 (1976); (c) L. Mandel and H. J. Kimble, Phys. Rev. A **15**, 689 (1977); (d) *Multiphoton Processes*, edited by J. H. Eberly and P. Lambropoulos (Wiley, New York, 1978); (e) J. L. F. de Meijere and J. H. Eberly, Phys. Rev. A **17**, 1416 (1978); (f) P. L. Knight, W. A. Molander, and C. R. Stroud, Jr., *ibid*. **17**, 1547 (1978); (g) S. N. Dixit, P. Zoller, and P. Lambropoulos, *ibid*. **21**, 1289 (1980); (h) P. Zoller, in *Multiphoton Processes*, edited by P. Lambropoulos and S. J. Smith (Springer, Berlin, 1986); (i) M. H. Anderson, R. D. Jones, J. Cooper, S. J. Smith, D. S. Elliott, H. Ritsch, and P. Zoller, Phys. Rev. A **42**, 6690 (1990); (j) A. H. Toor and M. S. Zubairy, *ibid*. **49**, 449 (1994).

[12] A. T. Georges, Phys. Rev. A **21**, 2034 (1980); R. E. Ryan and T. H. Bergeman, *ibid*. **43**, 6142 (1991).

[13] P. Zoller, Phys. Rev. A **19**, 1151 (1979); **20**, 1019 (1979); A. T. Georges, P. Zoller, and P. Lambropoulos, Phys. Rev. Lett. **42**, 1609 (1979); P. Zoller, G. Alber, and R. Salvador, Phys. Rev. A **24**, 398 (1981).

[14] G. Vemuri, R. Roy, and G. S. Agarwal, Phys. Rev. A **41**, 2749 (1990); G. Vemuri, K. V. Vasavada, and G. S. Agarwal, *ibid*. **50**, 2599 (1994).

[15] C. Cohen-Tannoudji and S. Reynaud, J. Phys. B **10**, 345 (1977); in *Multiphoton Processes* [Ref. [11(d)]], p. 103.

[16] H. J. Carmichael and D. F. Walls, J. Phys. B **9**, L43 (1976); H. J. Kimble and L. Mandel, Phys. Rev. A **13**, 2123 (1976); **15**, 689 (1977); H. J. Kimble, M. Dagenais, and L. Mandel, Phys. Rev. Lett. **39**, 691 (1977); F. Diedrich and H. Walther, *ibid*. **58**, 203 (1987); D. F. Walls and G. J. Milburn, *Quantum Optics* (Spring-Verlag, Berlin, 1994), Chap. 11, and references therein.

[17] M. Sargent III, Phys. Rep. **43**, 223 (1978); G. S. Agarwal, Phys. Rev. A **19**, 923 (1979); R. W. Boyd, M. G. Raymer, P. Narum, and D. J. Harter, *ibid*. **24**, 411 (1981).